Designing Metal-Organic Frameworks for Catalytic Applications

Liqing Ma and Wenbin Lin

Abstract Metal-organic frameworks (MOFs) are constructed by linking organic bridging ligands with metal-connecting points to form infinite network structures. Fine tuning the porosities of and functionalities within MOFs through judicious choices of bridging ligands and metal centers has allowed their use as efficient heterogeneous catalysts. This chapter reviews recent developments in designing porous MOFs for a variety of catalytic reactions. Following a brief introduction to MOFs and a comparison between porous MOFs and zeolites, we categorize catalytically active achiral MOFs based on the types of catalytic sites and organic transformations. The unsaturated metal-connecting points in MOFs can act as catalytic sites, so can the functional groups that are built into the framework of a porous MOF. Noble metal nanoparticles can also be entrapped inside porous MOFs for catalytic reactions. Furthermore, the channels of porous MOFs have been used as reaction hosts for photochemical and polymerization reactions. We also summarize the latest results of heterogeneous asymmetric catalysis using homochiral MOFs. Three distinct strategies have been utilized to develop homochiral MOFs for catalyzing enantioselective reactions, namely the synthesis of homochiral MOFs from achiral building blocks by seeding or by statistically manipulating the crystal growth, directing achiral ligands to form homochiral MOFs in chiral environments, and incorporating chiral linker ligands with functionalized groups. The applications of homochiral MOFs in several heterogeneous asymmetric catalytic reactions are also discussed. The ability to synthesize value-added chiral molecules using homochiral MOF catalysts differentiates them from traditional zeolite catalysis, and we believe that in the future many more homochiral MOFs will be designed for catalyzing numerous asymmetric organic transformations.

L. Ma and W. Lin (✉)
Department of Chemistry, University of North Carolina, CB#3290, Chapel Hill, NC 27599, USA
e-mail: wlin@unc.edu

Contents

Abbreviations

BDC   1,4-Benzenedicarboxylate acid
BET   Brunauer-Emmett-Teller
BINOL   1,1′-binaphthalene-2,2′-diol
BPDC   Biphenyl-4,4′-dicarboxylic acid
BTC   Benzene-1,3,5-tricarboxylate
MOFs   Metal-organic frameworks
SBU   Secondary building unit
TOF   Turn over frequency

# 1 Introduction

Metal-organic frameworks (MOFs), a new generation of hybrid materials built from organic bridging ligands and metal-connecting points, have received increasing attention over the past decade [1]. Much of the interest in MOFs arises from the tunability of such materials which allows their use in a number of applications [2–7]. One of the most extraordinary features of MOFs is their extremely high porosity. The resulting channels and cavities have sizes ranging from a few

Angstroms to several nanometers depending on the size of the ligands and the connectivity of the networks. The high porosity of MOFs has allowed their use in gas storage [8–11], most notably having shown promise in hydrogen storage which is one of the key hurdles for the future hydrogen economy.

The ability to incorporate catalytically active metal-connecting points or other functional groups into highly porous MOFs has allowed their applications in heterogeneous catalysis. Porous MOFs can be understood in analogy to the well-established microporous zeolites which have played a key role in catalytic processing of many important commodity chemicals. Zeolites are crystalline aluminosilicates constructed from interconnected SiO_4 and AlO_4 tetrahedra with charge-balancing organic and inorganic cations or protons. The resulting 3D frameworks are microporous with channels/cavities of up to 1.0 nm. These well-defined pore environments provide size- and shape-selectivity during the catalytic processes, and as such, zeolites have been widely used as selective catalysts in the petrochemical industry (such as fluid catalytic cracking and hydro-cracking). Such heterogeneous catalytic reactions improve gasoline quality, and significantly reduce the pollution from combustion engines.

Templating with different structure-directing agents (SDAs) has led to the synthesis of numerous zeolites with varied Si/Al molar ratios (and therefore varied acidity) and pore sizes and structures (Fig. 1). Such structural diversity is key to the processing of many organic molecules. However, the number of zeotypes is limited by the fixed tetrahedral coordination of the Si/Al connecting points and the oxide linker. It is also difficult to obtain zeolites with pore sizes larger than 1 nm, which limits the catalytic applications of zeolites to relatively small organic molecules (typically no larger than xylenes). Lastly, in spite of decades of research efforts, chiral
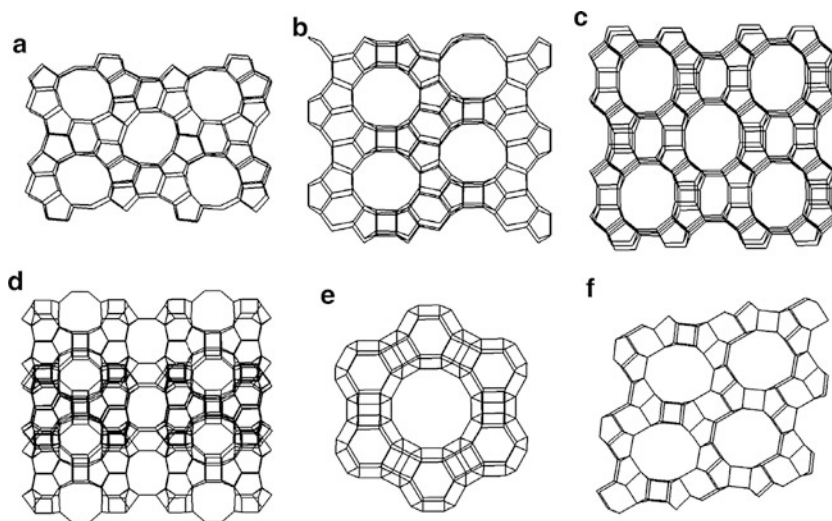

Fig. 1 Structures of zeolites ZSM-5 (**a**), mordenite (**b**), Beta (**c**), MCM-22 (**d**), zeolite Y (**e**), and zeolite L (**f**) (modified from [51])

zeolites still cannot be obtained in enantiopure form, which prevents applications of zeolites in catalytic asymmetric synthesis of value-added chiral molecules for the pharmaceutical, agrochemical, and fragrance industries.

Unlike zeolites that are built from interconnected tetrahedral aluminosilicates, MOFs can be constructed by linking a large variety of organic bridging ligands with many metal centers of diverse oxidation states and coordination geometries. Effectively, MOFs can be synthesized from an infinite number of metal/ligand combinations and thus have far greater diversity in structures, functional groups, and pore sizes and shapes. Greater tunability of porous MOFs should then allow for their use in catalytic reactions that cannot be realized with zeolites. Figure 2 exemplifies the structural tunability of MOFs. Para-aryl dicarboxylic acids of different lengths – 1,4-benzenedicarboxylate acid (BDC1,4-Benzenedicarboxylic acid), biphenyl-4,4′-dicarboxylic acid (BPDC) and *p*-terphenyl-4,4′-dicarboxylic acid – reacted with zinc(II) ions to lead to a series of isoreticular 3D porous MOFs. They are built from the same $Zn_4(\mu_4\text{-}O)(carboxylate)_6$ secondary building units (SBUs) which are further linked by dicarboxylate linkers to form cubic 3D networks. The pore and channel sizes of this family of isoreticular 3D MOFs can thus be readily tuned by simply adjusting the ligand length. The combination of a large inventory of organic bridging ligands and metal connectors has already led to numerous stable porous MOFs with a broad range of pore sizes and shapes.

Active catalytic sites in MOFs can be generated in several ways. First, the metal or metal cluster connecting points can be used to catalyze organic transformations. As shown in Scheme 1, a metal connecting point with a free coordinating site can be used as a Lewis acid catalyst after removal of coordinating solvent molecules from the axial positions of the metal center [12]. Metal cluster connecting points have also been used as active catalytic sites [13]. Second, active catalytic sites can be generated from the functional groups within a MOF scaffold (Scheme 2) [14, 15]. However, unlike traditional immobilized catalysts, the active catalytic sites generated in this fashion are arranged in a predictable and tunable manner due to the periodically ordered nature of the porous MOFs. Third, the catalytic activity of
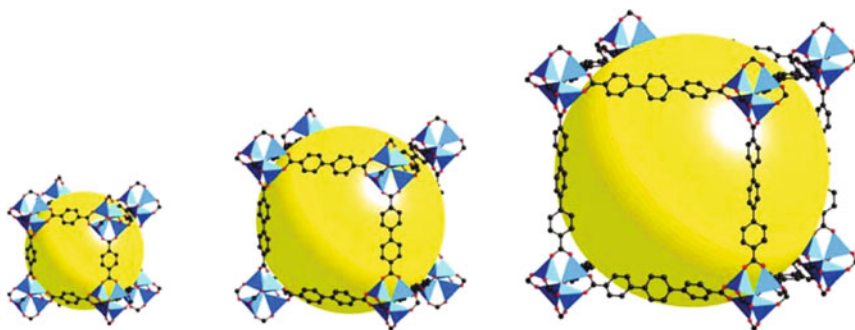
Fig. 2 MOFs constructed from linear dicarboxylate linkers showing different pore sizes as a result of different lengths of bridging ligands
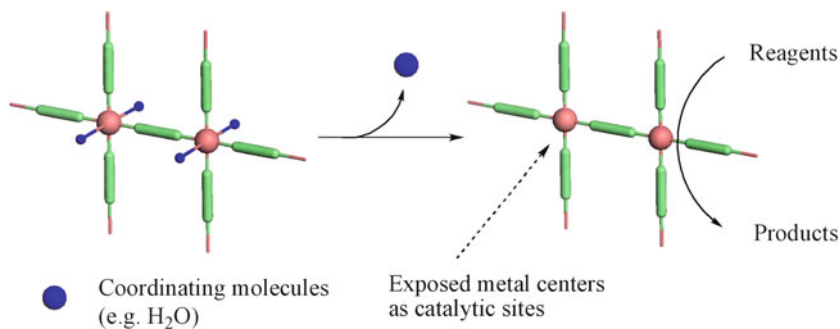
Scheme 1 Schematic illustrating the generation of unsaturated metal connecting points as active catalytic sites
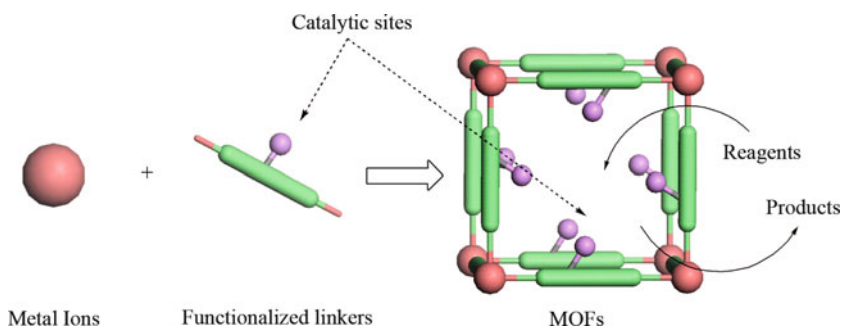
Scheme 2 Schematic showing the use of functional groups in the bridging ligands as active catalysts

MOFs can result from entrapped active catalysts, such as palladium or ruthenium nanoparticles (Scheme 3) [16, 17]. Finally, the pores and channels of MOFs can act as hosts with exquisite size selectivity for photochemical and polymerization reactions.

Among the many types of catalytic reactions, asymmetric catalysis is of great importance in industrial production of enantiomerically pure products. During the past few decades, much research effort has been devoted to the development of chiral zeolites and some other chiral porous materials having asymmetric catalytic sites. However, the traditional preparation procedures of zeolites require the removal of surfactant templates at the high temperatures of 400–550°C. Under such harsh conditions, the chirality of the preintroduced chiral surfactants, which are used to integrate silicate-surfactant assemblies into chiral conformations, is irreversibly destroyed. Therefore, an enantiomerically pure form of zeolite is not available to date. Compared to the syntheses of zeolites, homochiral MOFs can be
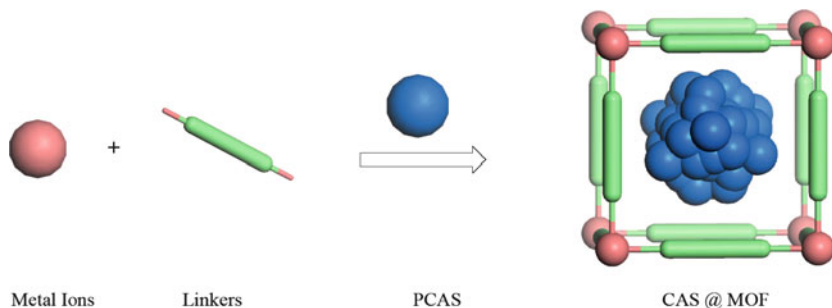
Scheme 3 Schematic representation of trapping catalytic active species (CAS) inside MOFs. (PCAS: precursor to CAS)

readily obtained under mild conditions and are expected to play an important role in heterogeneous asymmetric catalysis.

Although a very large number of MOFs have been reported in the past two decades, only a small number of them have been explored for catalytic applications. In this chapter we highlight recent developments in catalytically active MOFs. We first categorize achiral MOF catalysts based on the types of catalytic sites and organic transformations, followed by discussions on heterogeneous asymmetric catalysts based on homochiral MOFs.

2 Metal-Organic Frameworks as Achiral Catalysts

2.1 Metal Connecting Points in MOFs as Catalytic Sites

2.1.1 Cyanosilylation and Other Lewis Acid-Catalyzed Reactions

The metal-connecting points in MOFs often coordinate to labile solvent molecules or counter ions which can be replaced by organic substrates. The Lewis acidic nature of such metal centers can activate the coordinated organic substrates for subsequent organic transformations. Fujita and coworkers reported the first example of catalytically active MOFs based on this strategy in 1994 [18, 19]. When the linear bridging ligand 4,4′-bipyridine was treated with $Cd(NO_3)_2$, a colorless crystal with the composition of $[Cd(4,4′-byp)_2(H_2O)_2](NO_3)_2$ $4H_2O$ (**1**) was obtained. The Cd(II) centers in **1** adopt a distorted octahedral geometry by coordinating to four pyridines at the equatorial positions, and two water molecules in the axial positions to form a 2D infinite network (Fig. 3). The stacking pattern of such 2D layers is illustrated in Fig. 3b. The substrates can be hosted by the cavity of the first layer (space-filled), and further interact with the Lewis acid Cd(II) catalytic center in the

Fig. 3 Two dimensional
networks of **1** (**a**), and the
stacking pattern of two
adjacent layers of **1** (**b**) and
those layers were separated
by each other by a distance of
4.8 Å (**c**). Packing diagram of
**1** along *c* axis shows only
very small open channels (**d**)
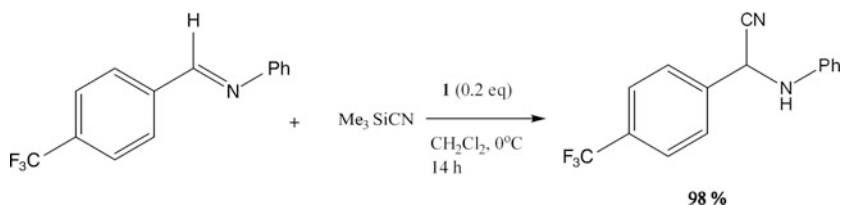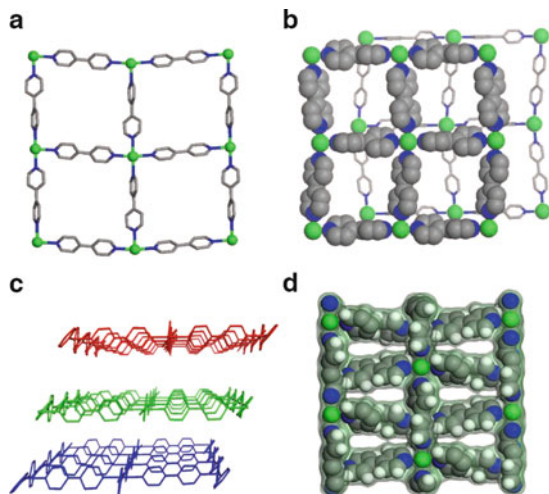
Scheme 4 Cyanosilylation of imines catalyzed by **1**

second layer (green ball). These layers are separated by an interlayer distance of
4.8 Å (Fig. 3c).

The activity of the Cd(II) centers in **1** as Lewis acid catalysts was illustrated by
cyanosilylation of aldehydes and imines. For the cyanosilylation of imines, most of
the reactions were complete within 1 h to afford aminonitriles in quantitative yield.
When the crystals were immersed in a CH_2Cl_2 solution with imines, there was no
detectable amount of entrapped imines in the solid, indicating that the open
channels of the frameworks were too small to accommodate imines used in the
reactions. It was thus suggested that the catalytic reactions might have exclusively
taken place on the surfaces of the crystals.

The authors took advantage of the much slower cyanosilylation rate of CF_3-
substituted imine to monitor the reaction process (Scheme 4). In order to prove that
the cyanosilylation was catalyzed by solid **1** heterogeneously, the solid catalyst was
filtered after 0.25 and 1 h of reaction, respectively. After the removal of the solid
catalyst, the reaction was not promoted any further, and the conversion remained at
21 and 59%, respectively (Fig. 4). The catalytic reactivity of **1** was further

Fig. 4 Conversion of CF$_3$-substituted imine catalyzed by **1**. Dash and dot lines indicate the conversion after filtration of solid **1** at 0.25 and 1 h
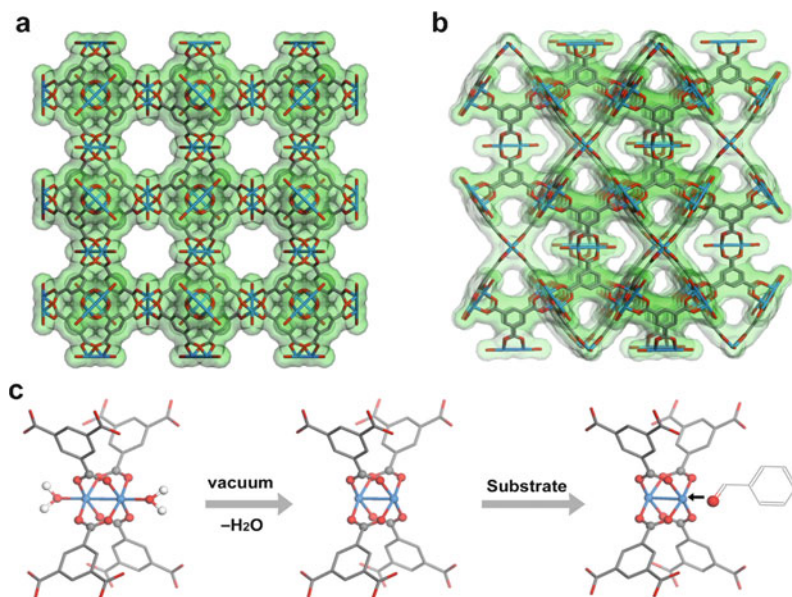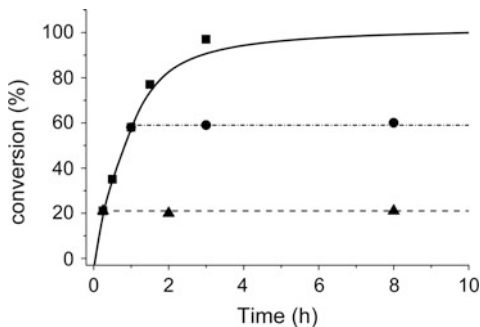
Fig. 5 Polymeric frameworks of **2** as viewed down the c axis (**a**) showing nanometer scale channels, and the projection on [101] plane (**b**); generation of the reagent accessible sites after dehydration of **2** (**c**)

compared with Cd(Py$_4$)(NO$_3$)$_2$ that bears the partial structure of **1**. Cd(Py$_4$)(NO$_3$)$_2$ promoted the reaction much less effectively, suggesting reaction rate enhancement in **1** as a result of stronger binding of the imine substrate to the hydrophobic grid cavities of **1**.

Kaskel and coworkers carried out similar cyanosilylation reactions with coordinatively unsaturated metal connecting points in 3D MOFs as heterogeneous catalysts [20]. The 3D framework [Cu$_3$(BTC)$_2$(H$_2$O)$_3$] (**2**) (BTC: benzene-1,3,5-tricarboxylate) used in this study was first reported by Williams et al. [21]. The open framework of **2** is built from dimeric cupric tetra-carboxylate units (paddlewheels) with aqua molecules coordinating to the axial positions and BTC bridging

ligands. The resulting frameworks possess channels of ~1 nm in size running through the [110] direction (Fig. 5a), and its porosity was confirmed by N_2 adsorption experiments which gave a Langmuir surface area of 918 m^2 g^{-1}, and a pore volume of 0.33 cm^3 g^{-1}.

As-synthesized **2** was first activated by heating at 373 K under vacuum to remove the H_2O molecules on the axial positions of the copper paddle wheels. The resulting coordinatively unsaturated Lewis acidic Cu(II) centers can coordinate to the aldehyde substrates to promote the cyanosilylation reaction (Fig. 5c). Activated **2** catalyzes the trimethylcyanosilylation of benzaldehydes with a very low conversion (<5% in 24 h) at 293 K. As the reaction temperature was raised to 313 K, a good conversion of 57% with a selectivity of 89% was obtained after 72 h. In comparison, less than 10% conversion was observed for the background reaction (without **2**) under the same conditions. The heterogeneous nature of this catalyst system was demonstrated by removing the solid from the reaction mixture after 8 h of initial reaction (8% conversion at this point). The conversion of the colorless filtrate did not increase any further after the removal of the solid catalyst.

The limitation of MOFs as heterogeneous catalysts was revealed in this study. First, the decomposition of the framework of **2** became apparent as the reaction temperature was raised above 333 K due to the reduction of Cu(II) to Cu(I) by aldehydes. Second, strong solvent inhibition effect was also observed. Electron-donating solvents such as THF competed with aldehydes for coordination to the Cu (II) sites, and no cyanosilylation product was observed in these solvents. Finally, the framework of **2** was not stable in some organic solvents, as demonstrated by the decomposition of **2** in CH_2Cl_2 even at room temperature. As a result, **2** gave the best activity for cyanosilylation of aldehydes in nonpolar solvents such as pentane in a limited temperature range.

Several other groups have also reported the use of metal-connecting points in MOFs as catalysts. For example, Lin and coworkers reported a series of lanthanide phosphonates possessing both Lewis and Brönsted acid sites that were capable of catalyzing cyanosilylation of aldehydes and ring opening of *meso*-carboxylic anhydrides [12]. These materials exhibit lamellar structures that can swell to facilitate the access of substrates with a wide range of dimensions. Long and coworkers reported a rigid 3D MOF with exposed Mn(II) centers residing in the open channels [22]. These Lewis acidic sites effectively catalyzed the cyanosilylation with a high level of size-selectivity due to the rigid 3D framework structure. The previously mentioned [Cu$_2$(BTC)$_2$] was also reported as a Lewis acid catalyst for the isomerization of terpene derivatives [23].

2.1.2 Oxidation of Alcohols, Thiols, and Thio Ethers

The electron-deficient nature of some metal-connecting points and clusters makes the resulting MOFs efficient oxidation catalysts. It is well established that binuclear copper complexes can be used as oxidation catalysts with oxygen or H_2O_2 as the oxidant [24]. Mori and coworkers reported MOFs with [Cu$_2$(OOCR)$_4$]
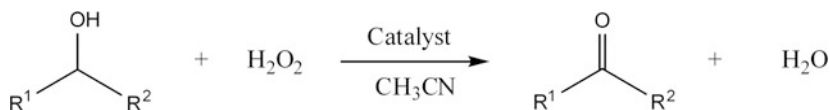
Scheme 5 Catalytic oxidation of alcohols by hydrogen peroxide
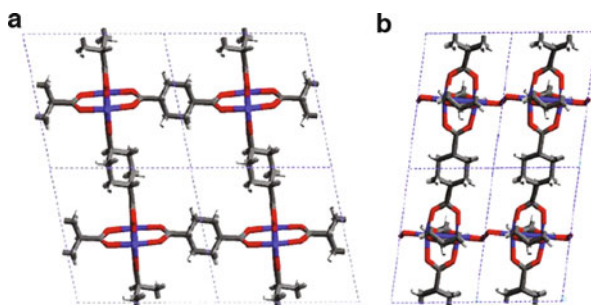
Fig. 6 (**a**) 2D structure of **3**, viewed along c axis. (**b**) Structure of frameworks **4**, viewed along the b axis, showing linking of 2D networks by the peroxo groups. (modified from [25])

paddle wheel units as heterogeneous catalysts for the oxidation of alcohols (Scheme 5) [25].

The 2D framework $[Cu_2(O_2CC_6H_{10}CO_2)_2]$, **3**, was synthesized by reacting 1, 4-cyclohexanedicarboxylic acid with a copper(II) salt. The 2D framework structure in **3** is built form linking the $[Cu_2(OOCR)_4]$ paddle wheel units with *trans*-1, 4-cyclohexanedicarboxylate bridging ligands. Addition of H_2O_2 to the suspension of frameworks **3** led to green copper peroxo framework **4**. Upon forming the peroxo complex **4**, 2D layers of $[Cu_2(O_2CC_6H_{10}CO_2)_2]$ grids were linked by the 1,2-*trans*-Cu-O-O-Cu species to form a 3D framework structure (Fig. 6).

The porosity of the complexes **3** and **4** was characterized by N_2 adsorption experiments. The adsorption isotherms showed typical Langmuir type isotherms, indicating the presence of micropores in both **3** and **4**. Analyses of the adsorption isotherms revealed the same effective pore diameter of 4.9 Å in both frameworks, and a BET surface area of 393.9 m^2 g^{-1} and 328.4 m^2 g^{-1} for **3** and **4**, respectively.

The catalytic activity of complex **3** was investigated by carrying out alcohol oxidation with H_2O_2 as the oxidant (Table 1). Complex **3** catalyzed the oxidation of primary alcohol, secondary alcohol and benzyl alcohols with high selectivity. The oxidation of 2-propanol showed faster reaction rate and higher conversion than that of cyclohexanol. Such a difference might be attributed to the smaller size of 2-propanol which made it easier to enter the cavities of the microporous framework. In terms of reaction mechanism, complex **4** could be considered as an active intermediate during the reaction process catalyzed by **3**. This assumption was confirmed by the detection of ketone when treating alcohols with **4** in the absence of H_2O_2.

**Table 1** Oxidation of alcohol with H_2O_2 catalyzed by **3***

Entry	Substrate	Selectivity (%)	TOF (s^{-1})	Conversion (%) (h)
1[a]	2-Propanol	Acetone (>99%)	1.6×10^{-3}	17.1 (1)
2[b]	2-Propanol	Acetone (>99%)	5.8×10^{-3}	55.6 (3)
3[c]	Cyclohexanol	Cyclohexanone (>99%)	1.1×10^{-4}	14.3 (168)
4[b]	Cyclohexanol	Cyclohexanone (>99%)	1.6×10^{-4}	19.8 (168)
5[a]	Benzylalcohol	Benzaldehyde (>99%)	7.0×10^{-4}	16.7 (144)
6[b]	Benzylalcohol	Benzaldehyde (>99%)	1.5×10^{-3}	25.8 (144)
7[a]	1-Octanol	Octylaldehyde (>99%)	1.1×10^{-4}	10.8 (168)
8[b]	1-Octanol	Octylaldehyde (>99%)	1.6×10^{-4}	13.2 (168)

*Excess of H_2O_2 was used
[a]23-fold
[b]113-fold
[c]46-fold
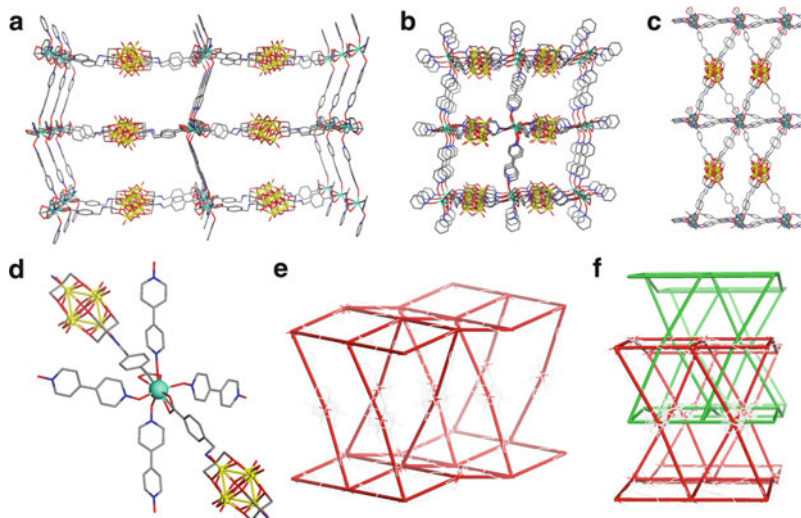
Fig. 7 2D sheets of Tb(III) centers interconnected by bpdo linkers leading to 3D networks **5** as viewed down the *a* axis (**a**); *b* axis (**b**) and *c* axis (**c**). (**d**) Tb coordination environment in **5**. (**e**) Simplified schemes of the networks (onefold shown) of **5**. (**f**) Schematic representation of the twofold interpenetrating networks of **5**

Hill et al. have demonstrated the sulfoxidation of thioethers using an MOF based on vanadium-oxo cluster V_6O_{13} building units [13]. The 3D MOF Tb $[V_6O_{13}\{(OCH_2)_3C\text{-}(NHCH_2C_6H_4\text{-}4\text{-}CO_2)_2\}\{bpdo\}_2]$, (**5**, bpdo = 4,4′-bis(pyridine-N-oxide)) was prepared by slow diffusion between $Tb(NO_3)_3$ and bpdo/ $[V_6O_{13}\{(OCH_2)_3C\text{-}(NHCH_2C_6H_4\text{-}4\text{-}CO_2)\}_2]^{4-}$ (**V-1**). Compound **5** is built from linking 2D grids comprising Tb(III) centers and bpdo units by **V-1** into the 3D framework. Two independent 3D networks in **5** interpenetrate to lead to

$$R\text{-}SH \quad + \quad O_2 \quad \xrightarrow{\text{cat. (5)}} \quad R\text{-}SS\text{-}R \quad + \quad H_2O$$
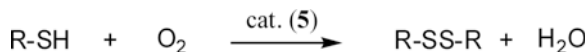
Scheme 6 Oxidation of thiols catalyzed by **5**

microporous channels with the dimensions of 8.0×5.2 Å along the crystallographic *a*-axis (Fig. 7).

The vanadium oxide clusters in **5** showed catalytic activity in the sulfoxidation of thioethers or thiols (Scheme 6). When *tert*-butylhydroperoxide (TBHP) was used as an oxidant, tetrahydrothiophene (THT) was oxidized much faster with **5** than in the control experiment without **5**. More importantly, such sulfoxidation could be performed with **5** as catalyst using ambient air as oxidant. However, formation of the desired product dipropylsulfane (PrSSPr) was very slow, and a 41% yield was obtained after 30 days at 45°C.

Several other MOFs have also been used as oxidation catalysts. Kim and coworkers used [Zn$_2$(BDC)(*L*-Lac)(DMF)]·DMF as a heterogeneous catalyst for the oxidation of thioethers to sulfoxides by urea hydroperoxide (UHP) or hydrogen peroxide (H$_2$O$_2$) [26]. Its size selectivity was illustrated by the higher conversion of smaller sulfides over larger ones. Snejko and coworkers reported the use of In$_2$(OH)$_3$(BDC)$_{1.5}$ [27] and [Sc$_2$(BDC)$_3$] [28] as active catalysts for the oxidation of alkylphenylsulfides.

2.2 MOFs Containing Functional Linkers as Catalytic Sites

2.2.1 Amide-Catalyzed Knoevenagel Condensation Reactions

In many MOFs, all of the coordination sites around the metal centers are occupied by linker ligands, and it is difficult to use the metal connecting points as catalytic sites in these materials. An alternative strategy in this case is to exploit the functional groups on the linker ligands for potential catalytic activities. In order to construct such catalytically active MOFs, the functional groups in the linker ligands must be able to sustain the conditions used for synthesizing the frameworks or can be regenerated in the postmodification of the frameworks. The functional groups within the resulting frameworks must be accessible to the reagents through the open channels. Kitagawa and coworkers reported a 3D MOF {[Cd(4-btapa)$_2$(NO$_3$)$_2$]·6H$_2$O·2DMF} (**6**, 4-btapa = 1,3,5-benzene tricarboxylic acid tris [*N*-(4-pyridyl)amid]) constructed by tridentate amide linkers and cadmium salt [14]. The pyridine groups on the ligand 4-btapa act as ligands binding to the octahedral cadmium centers, while the amide groups can provide the functionality for interaction with the incoming substrates (Scheme 7). Specifically, the – NH moiety of the amide group can act as electron acceptor whereas the –C=O group can act as electron donor to activate organic substrates for subsequent reactions.
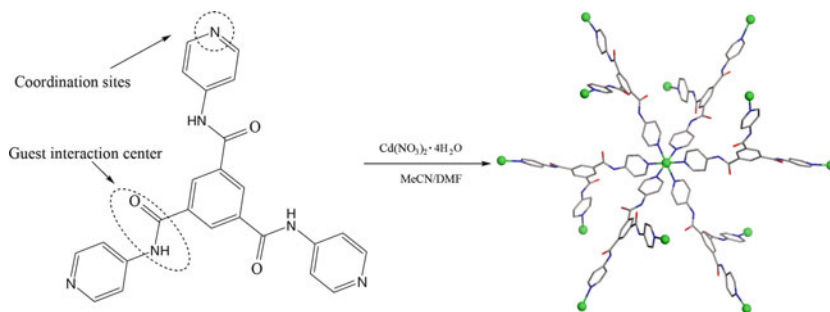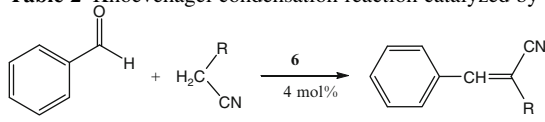
Scheme 7 Synthetic scheme for MOFs that contain amide groups in the bridging ligands
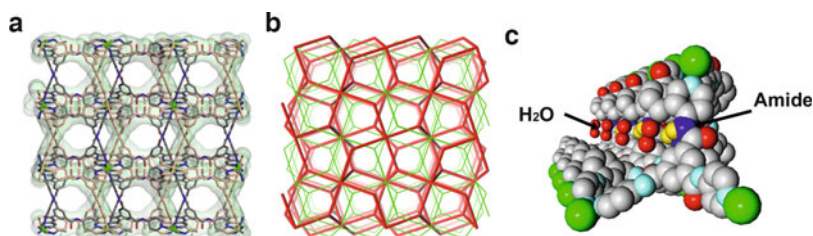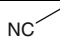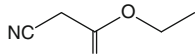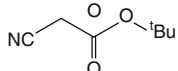

Fig. 8 Twofold interpenetrating structure of **6** showing 3D channels of dimensions of 4.7 × 7.3 Å (**a**), and its simplified scheme (**b**). (**c**) View of ordered amide groups facing the open channels of **6**, with H_2O molecules binding to –NH group through hydrogen bonding

Compound **6** adopts a twofold interpenetrating framework structure with free amide groups pointing towards to the open channels (Fig. 8). The resulting zigzag channels with dimensions of 4.7 × 7.3 Å are occupied by nitrate anions, water and DMF molecules.

The amide groups in **6** were used as weak bases to catalyze Knoevenagel condensation reactions of benzaldehyde with cyano compounds. Three cyano compounds with different sizes, malononitrile, ethyl cyanoacetate, and cyano-acetic acid *tert*-butyl ester, showed very different results. The smallest substrate, malononitrile, gave 98% conversion of the addition product, while the largest one, cyano-acetic acid tert-butyl ester, gave no conversion at all (Table 2). Such a guest-selective reaction indicated that the reaction was catalyzed inside the crystal channel instead of the surface. Much slower reaction and lower conversion were observed both for the desolvated sample of **6** and for the free ligand 4-btapa. In the desolvated sample of **6**, there is no porosity for the substrates to interact with the amide groups residing inside the solid, whereas the amide groups in the free ligand 4-btapa form intermolecular hydrogen bonds with each other and are thus not available to activate the cyano compounds for Knoevenagel condensation reactions.

Table 2 Knoevenagel condensation reaction catalyzed by **6**

Run	Substrate	Molecule size	Conversion (%)
1	NC⌒CN	4.5×6.9 Å	98
2	NC⌒C(O)OEt	4.5×10.3 Å	7
3	NC⌒C(O)O-^{t}Bu	5.8×10.3 Å	0

All of these experimental observations are consistent with the heterogeneous nature of **6** as a weak base catalyst for Knoevenagel condensation reactions.

2.2.2 Grafting of Catalytically Active Functional Groups to the Unsaturated Metal Sites

Catalytically relevant functional groups can also be introduced by grafting onto unsaturated metal sites within MOFs. Ferey et al. reported a robust and highly porous MOF $[Cr_3(\mu_3\text{-}O)F(H_2O)_2(BDC)_3]$ (**7**) constructed from BDC and chromium (III) nitrate (also called MIL-101) [16, 29]. In situ IR spectroscopic studies via CO adsorption indicated that **7** has a number density of unsaturated Cr(III) sites of 1.0 mmol g^{-1}. Instead of directly using the unsaturated Cr(III) centers as catalytic sites, the authors grafted ethylenediamine (ED) onto the Cr(III) sites (Fig. 9c). **7** has
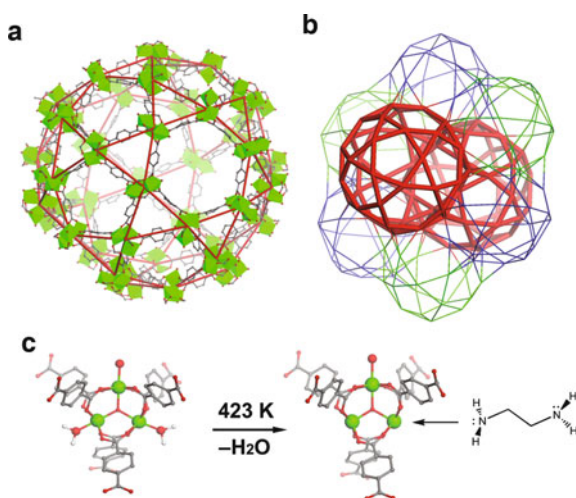
Fig. 9 (**a**) Perspective view of mesoporous cage of **7** showing hexagonal windows. (**b**) Two types of super cages, *red* and *green/blue*, representing the highly porous zeolite-type MOF 7. (**c**) Evolution of unsaturated chromium centers by removal of the bounding water molecules, and its accessibility to ethylenediamine (ED) molecules

an extremely high Langmuir surface area of 5900 m^2 g^{-1} owing to its zeolite-type structure having extraordinary large cages with diameters of 2.9 and 3.4 nm (Fig. 9a, b). Although ED takes up some of the space within the frameworks, the nitrogen uptake experiments still showed a large Langmuir surface area of 3555 m^2 g^{-1} for the ED-grafted **7**. As the uncoordinated ends of ED can act as base catalytic sites, ED-grafted **7** was tested for Knoevenagel condensation reactions. A significant increase in conversion was observed for ED-grafted **7** as compared to untreated framework **7** (98% vs 36%).

## 2.3 Entrapment of Catalytically Active Noble Metal Nanoparticles

Since the porosity and crystallinity of **7** were well maintained after ED grafting, the uncoordinated end of ED provides a site for further modification via encapsulation of noble metals. After being treated with aqueous HCl solution, the positively charged ammonium groups (from protonated ED) interacted with noble metal salts, such as $[PdCl_4]^{2-}$, which was later reduced into noble metal by NaBH$_4$. The resulting Pd nanoparticles entrapped into the framework for example showed similar catalytic activity as Pd/C in Heck coupling reactions.

With a similar approach, Fischer and coworkers entrapped Ru nanoparticles inside porous [Zn$_4$O(BDC)$_3$] (MOF-5) by hydrogenolysis of the adsorbed volatile ruthenium species [Ru(COD)(COT)] (COD = 1,5-cyclooctadiene, COT = 1,3,5-cyclooctatriene) [17]. The included Ru nanoparticles had a size range of 1.5–1.7 nm, and the intact framework of MOF-5 was confirmed by different spectroscopic methods. The resulting solid Ru@MOF-5 was tested for oxidation of benzyl alcohol; however, only a modest conversion of 25% to benzyl aldehyde was obtained, and the XRD revealed the breakdown of the structure of MOF-5 as well as the loss of framework porosity. In contrast, the crystallinity of Ru@MOF-5 remained when it was used to catalyze the hydrogenation of benzene to cyclohexane with 25% conversion under 3 bar H$_2$ at 75°C (Scheme 8).

2.4 MOFs as Reaction Hosts with Size Selectivity

2.4.1 Reaction Host for Photochemical Synthesis

Due to the highly ordered structures of MOFs, pores of specific sizes and shapes can be purposely constructed and used as nano-reactors for size-selective reactions. Li and coworkers synthesized a 3D MOF [Co$_3$(bpdc)$_3$(bpy)]·4DMF·H$_2$O (**8**, bpdc: biphenyldicarboxylate, bpy: 4,4′-bipyridine) by a solvothermal reaction of 1-D polymer [Co(bpdc)(H$_2$O)$_2$]·H$_2$O and 4,4′-bipyridine [30]. The resulting twofold interpenetrating 3D porous framework (Fig. 10) showed great thermal stability. The
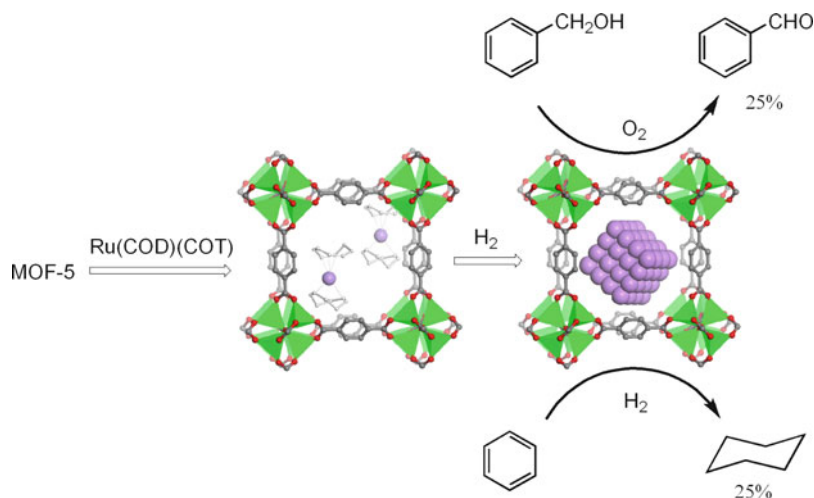
Scheme 8 Schematic for the formation of Ru@MOF-5 and its applications on alcohol oxidation and benzene hydrogenation
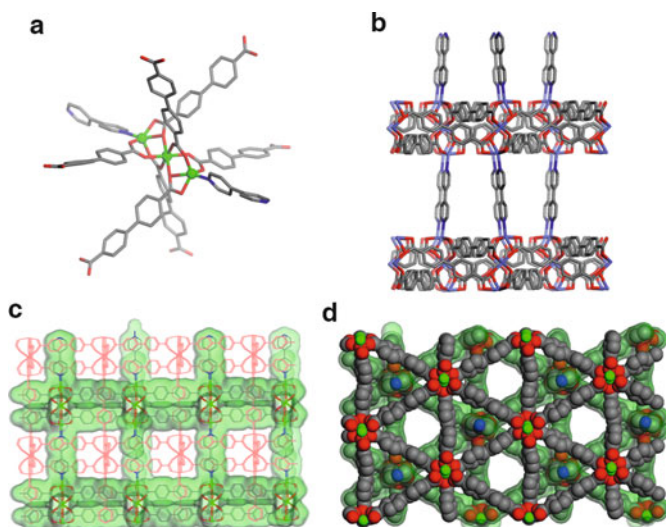
Fig. 10 (**a**) Coordination environment of Co, showing the building unit of $[Co_3(bpdc)_3(bpy)]$ (**8**). (**b**) Packing diagram of one of the two nets of **8** viewed down the *b* axis. (**c**) Twofold interpenetrating 3D networks viewed down the *a* axis. (**d**) Space-filled model of **8** viewed perpendicular to the (001) plane

framework structure remained essentially unchanged even after evacuating the pristine sample at 300°C.
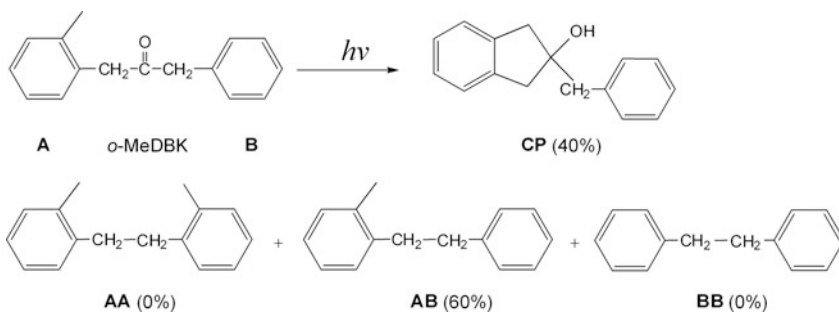
Scheme 9 Schematic illustration photoreaction of *o*-MeDBK
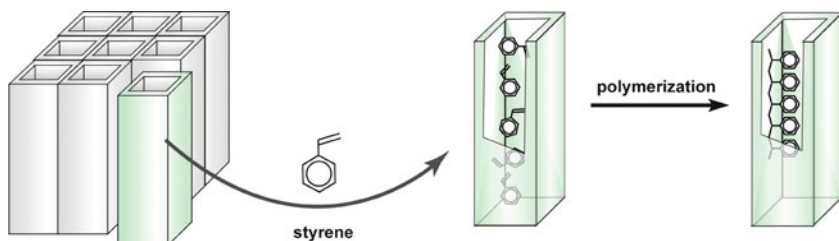
Fig. 11 Schematic illustration of styrene polymerization in the 1-D channels within the MOFs (courtesy of Professor Kitagawa)

Further analysis of the channels of **8** shown in Fig. 10d revealed the existence of supercages with the size of $11 \times 11 \times 5$ Å, which are interconnected through narrower windows with a maximum dimension of 8 Å. The supercages and channels in **8** were tested as hosts for size-selective reactions. The photochemistry of *o*-methyl dibenzyl ketone (*o*-MeDBK) was examined utilizing **8** as the reaction host (Scheme 9). This type of photochemical reactions was extensively studied using FAU and MFI zeolites as hosts [31]. During the photoreaction, the *o*-MeDBK in the singlet state can undergo intramolecular hydrogen abstraction followed by cyclization to produce cyclopentanol, **CP**. On the other hand, α cleavage followed by decarbonylation forms a geminate pair of hydrocarbon radicals, which randomly recombine to afford products **AA**, **AB**, and **BB**. The photolysis of *o*-MeDBK in the presence of **8** produced CP in 40% yield along with the single radical recombination product **AB** in 60% yield. The exclusive production of **AB** was rationalized by a "cage effect" of 100% efficiency (for comparison, the same photolysis in NaX has a cage effect of 70%). Only 50% of the overall product could be extracted from the solid. The remaining product had to be recovered by breaking down the framework **8** via soaking in water. 1-D compound $[Co(bpdc)(H_2O)_2] \cdot H_2O$ could be recycled after breaking down **8**.
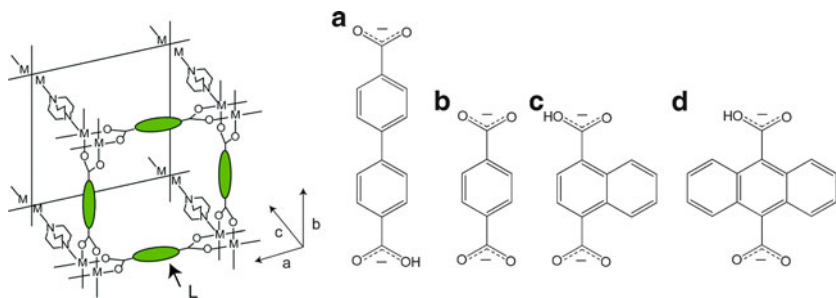
Fig. 12 Combination of different metal (Cu^{2+} or Zn^{2+}) with different size of linker ligands **L** (**a–d**) to result in 3D MOF with open channels along the *c* axis

Table 3 Polymerization of styrene in nanochannels of **9** and **10** at 70°C for 48 h

Host (pore size [Å]^2	Adsorbed monomer (number/unit cell)	Conversion (%)	$M_n(M_w/M_n)$
9a (10.8 × 10.8)	3.1	81	14,000 (3.3)
9b (7.5 × 7.5)	2.5	71	54,600 (1.6)
9c (5.7 × 5.7)	2.2	58	10,100 (1.6)
9d (4.8 × 4.3)	1.6	0	
10b (7.5 × 7.5)	2.5	71	56,200 (1.7)
10c (5.7 × 5.7)	2.1	56	11,100 (1.5)
10d (4.8 × 4.3)	1.6	0	
Bulk polymerization			37,600 (4.7)

2.4.2 Reaction Host for Polymerization

Certain types of reactions, such as polymerization, in the confined nanoscale channels/space may have different pathways compared with those in open space. Kitagawa and coworkers have utilized size-tunable MOFs as reactions hosts for radical polymerization of activated monomers, such as styrene, divinylbenzene, substituted acetylenes, methyl methacrylate, and vinyl acetate (Fig. 11) [32–35]. *Para*-dicarboxylate linkers of different sizes, **a–d**, were used to link Cu^{2+} and Zn^{2+} centers to form 2D sheets which were further linked by triethylenediamine to form 3D frameworks **9a–d** (for Cu^{2+}) and **10b–d** (for Zn^{2+}) that possess 1-D channels (Fig. 12).

Owing to the different size of linker ligands **a–d**, the resulting frameworks possessed open channels of varied sizes from 4.3 × 4.8 Å^2 to 10.8 × 10.8 Å^2. Polymerization of styrene was performed using **9a–d** and **10b–d** as hosts at 70°C. Since styrene has a slightly larger dimension than the channels in **9d** and **10d**, as expected, no conversion was observed when these two frameworks were used (Table 3). Most importantly, the molecular weight distribution (i.e., polydispersity index M_w/M_n) of polystyrenes produced within the nanochannels was narrower than

those prepared by bulk synthesis. This unique capability of molecular weight control was further examined by ESR measurement. Intense signals assigned to the propagating radicals of polystyrene were observed, reaching 2.6 mmol kg^{-1} in **10b**, which is significantly higher than those detected in conventional solution radical polymerizations (10^{-4}–10^{-5} mmol kg^{-1}). The nanochannels could thus better stabilize the propagating radicals and suppress the termination reactions, leading to smaller and more desirable M_w/M_n values.

3 Homochiral MOFs as Asymmetric Catalysts

## 3.1 General Strategies for Homochiral MOF Synthesis

As illustrated in cyanosilylation and other lewis acid-catalyzed reactions, applications of MOFs in achiral catalysis suffer from several limitations when compared with traditional inorganic oxide catalysts, including limited thermal and hydrolytic stabilities. It will thus be difficult for MOFs to compete against zeolites for the reactions that require high temperatures and aggressive solvents. On the other hand, no known zeolites can be used to catalyze enantioselective reactions. Given that most asymmetric catalytic reactions are carried out in nonaggressive solvents under mild conditions, MOFs appear to be ideally suited for such applications owing to the ability to prepare chiral MOFs with large open channels in a modular fashion.

Compared to relatively few examples of MOF-based achiral catalysts, there are even fewer examples of homochiral MOFs used in asymmetric catalytic reactions. Several distinct strategies can be used to construct homochiral MOFs. Ideally, crystallization of homochiral MOFs via self-resolution from achiral linker ligands is the most economical way to accomplish such a goal. However, the resulting bulk samples, in almost all of the cases, contain both enantiomorphs and are thus racemic. Aoyama and coworkers successfully obtained homochiral MOFs in the bulk from achiral ligands by carefully controlling nucleation in the crystal growth process [36]. Zheng and coworkers recently reported the synthesis of homochiral MOFs from achiral ligands by chemically manipulating the statistical fluctuation of the formation of enantiomeric pairs of crystals [37]. Growing MOF crystals under chiral influences is another approach to obtain homochiral MOFs using achiral linker ligands. Rosseinsky and coworkers have introduced a chiral coligand to direct the formation of homochiral MOFs by controlling the handedness of the helices during the crystal growth [38, 39]. Morris and coworkers utilized ionic liquid with chiral cations as reaction media for synthesizing MOFs, and successfully obtained homochiral MOFs even though they do not contain cationic part of the ionic liquid [40]. The most reliable strategy for synthesizing homochiral MOFs is, however, to use the readily available chiral linker ligands for their construction. A number of homochiral MOFs with open framework structures were synthesized

by this method in recent years [41–46]. All of the homochiral MOFs examined for asymmetric catalytic reactions so far have been made using this strategy.

3.2   Homochiral MOFs with Interesting Functionalities and Reagent-Accessible Channels

Although a number of chiral building blocks can be used to construct homochiral MOFs, Lin and coworkers focused on enantiopure 1,1′-binaphthyl-derived linker ligands because the related 1,1′-bi-2,2′-naphthol (BINOL) and 2,2′-bis(diphenyl-phosphino)-1,1′-binaphthyl (BINAP) are among the most widely used chiral ligands for homogeneous asymmetric catalysis [47, 48]. They have successfully constructed homochiral MOFs using 1,1′-binaphthyl-derived chiral bridging ligands containing orthogonal functional groups that can be used to coordinate to catalytically active metal centers to enhance enantioselectivity. One of the advantages of using the 1,1′-binaphthyl moiety as the chiral backbone is the ability to
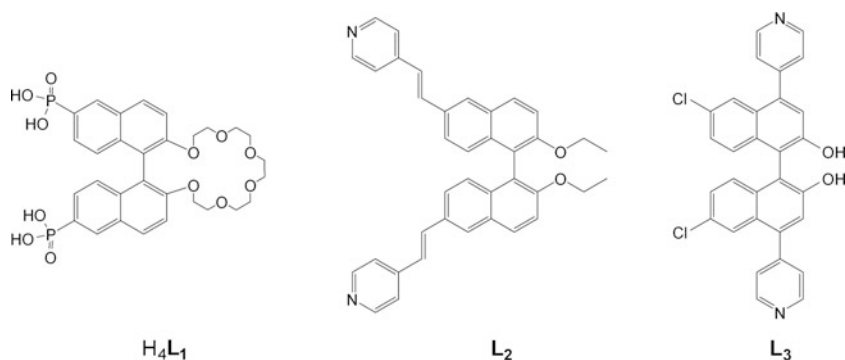

Scheme 10 Homochiral bridging ligands derived from BINOL
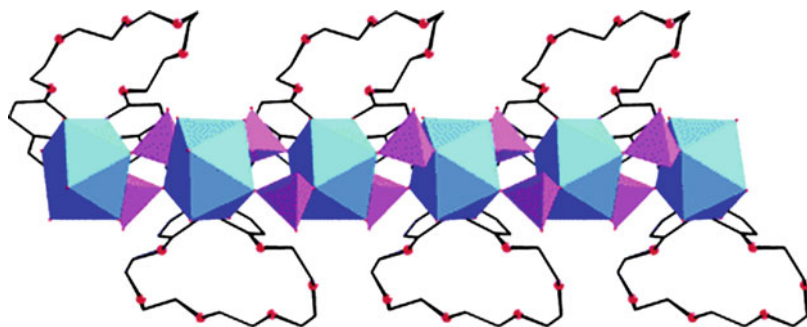
Fig. 13 Chiral crown ether pillars on lamellar lanthanide bisphosphonate **11**

selectively functionalize at specific positions. As shown in Scheme 10, a variety of linking groups such as pyridine, phosphonic acid, and carboxylic acid can be selectively introduced to the 3,3′, 4,4′, and the 6,6′ positions of the 1,1′-binaphthyl moiety. Moreover, the length of the linker groups can be readily adjusted in order to tune the framework structure and porosity of the resulting materials.

The Lin group has prepared a number of homochiral MOFs based on 1,1′-binaphthyl-derived bridging ligands that contain additional functional groups for potential enantioselective recognition and separation processes. For example, homo-chiral lanthanide bisphosphonate MOF $[Ln_2(H_2L_1)_2(CH_3OH)]\cdot H_4L\cdot 3HCl\cdot 6H_2O$ (**11**) was built from chiral bridging ligand L_1 containing crown ether groups (Fig. 13) [42], which are potentially useful in bulk chiral separation of racemic ammonium salts (such as protonated amino acid derivatives). Although these lamellar solids maintained their framework structures after the removal of guest molecules, the limited porosity has precluded their application in enantioselective separations.
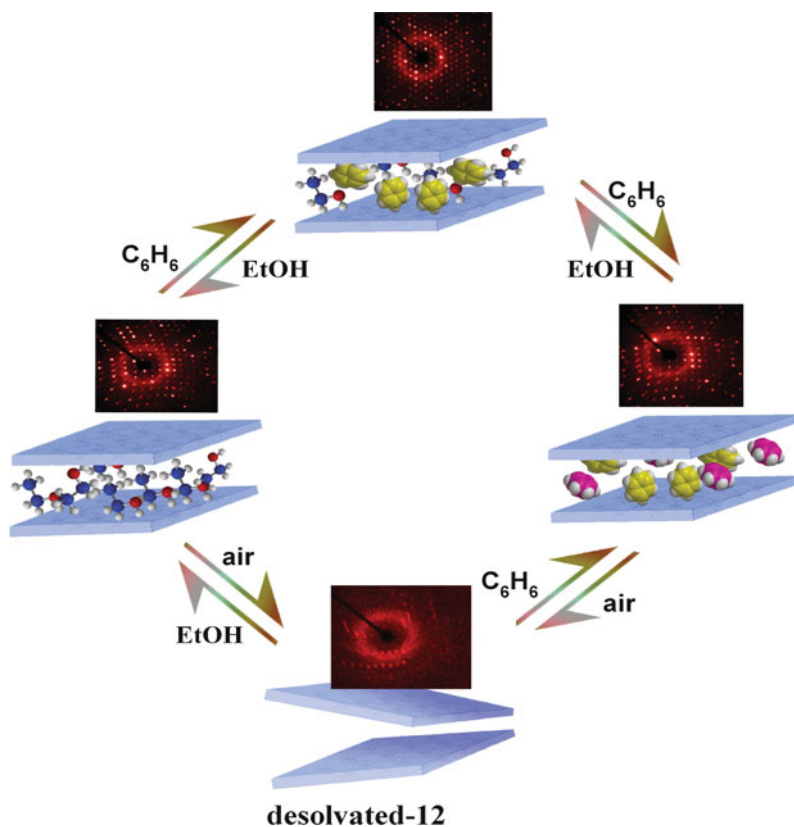

Fig. 14 Schematic representation of the reversible single-crystal to single-crystal and single-crystal to amorphous to single-crystal transformation processes of **12**

An effective MOF-based heterogeneous asymmetric catalyst needs to satisfy two requirements: the ability to maintain the framework structure under catalytic conditions and the facile transport of the reagents and products through the open channels in order for the substrates to access the active catalytic sites. Increasing the length of the bridging ligands may be a feasible way to create more solvent/reagent accessible channels built with the frameworks. However, longer bridging ligands may lead to framework catenation which will reduce the pore size [9]. Another undesired effect caused by the longer bridging ligands is the framework distortion after the removal of guest molecules. In order to probe the feasibility of designing homochiral MOFs that satisfy both of these requirements, Lin et al. synthesized a highly porous homochiral MOF $[Cd(L_2)_2(ClO_4)_2]\cdot11EtOH\cdot6H_2O$ (**12**) based on 1-D coordination polymers that were built from linking $Cd(ClO_4)_2$ with the elongated di-pyridyl ligand **L_2** [43]. Compound **12** can readily exchange solvent molecules upon exposing the pristine crystals to a vapor of other solvents, and interestingly, the solid underwent single-crystal-to-single-crystal transformation during the solvent exchange processes. The pristine solid lost crystallinity upon removal of the solvent molecules in air, but the crystallinity was regained upon exposure the amorphous solid to solvent molecules (Fig. 14). These results suggest that the framework structures of homochiral MOFs can be maintained during potential heterogeneous asymmetric catalytic reactions and true heterogeneous asymmetric catalysts can be built from homochiral MOFs.
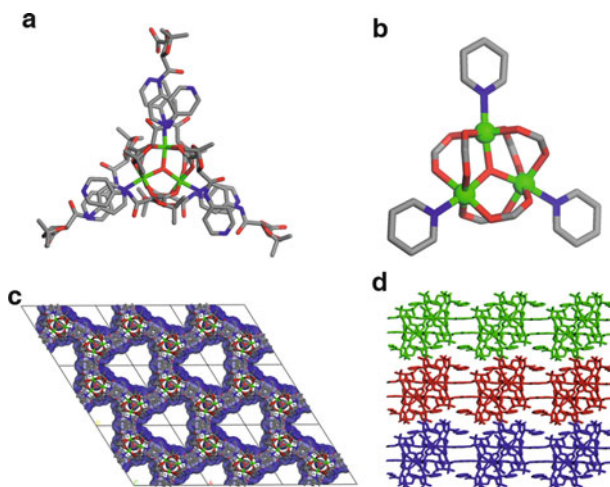
Fig. 15 (**a**) $[Zn_3(\mu\text{-}O)(L_4)_6]$ SBUs in (**13**). (**b**) Coordination environment or metal centers of **13**. (**c**) Large 1-D equilateral triangular shape channel along the *c* axis, with a size of 13.4 Å. (**d**) Stacking patterns of 2D layers (depicted in *different colors*) as viewed along the *a* axis
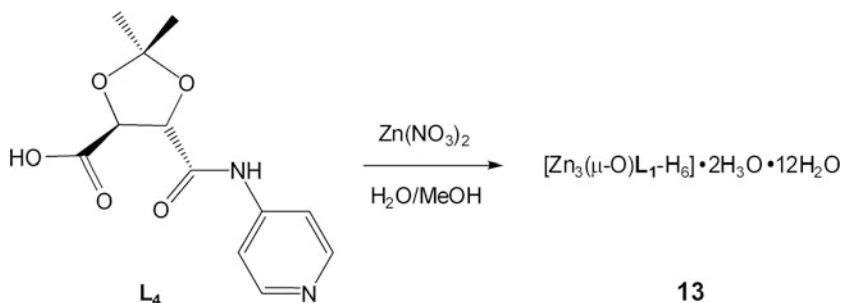
Scheme 11 Synthesis of homochiral **13**
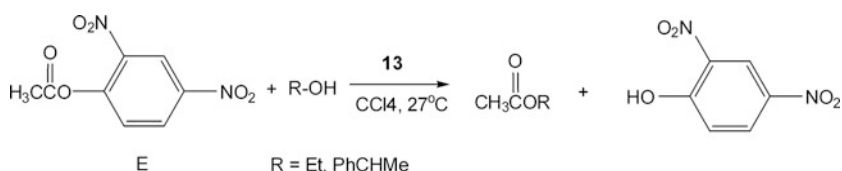
Scheme 12 Transesterfication of esters catalyzed by **13**

## 3.3 Nonchiral Active Sites Within the Homochiral Framework Structures

Kim and coworkers reported the first example of asymmetric catalysis using a homochiral MOF, albeit with a very modest enantioselectivity (ee) [41]. Chiral porous $[Zn_3(\mu_3\text{-O})(L_4\text{-H})_6]\cdot 2H_3O\cdot 12H_2O$ (**D-POST-1**, or **13**) was synthesized from a solvothermal reaction of $Zn(NO_3)_2$ and enantiopure chiral ligand **L_4** which is from readily derived from D-tartaric acid (Scheme 11). The oxo-bridged zinc trinuclear unit in **13** is coordinated by six carboxylate groups to form a SBU, which is further interconnected through zinc ions and pyridyl groups to result in large chiral 1D channels of ~13.4 Å along the *c* axis (Fig. 15).

Each trinuclear zinc unit contains six pyridyl groups, three of which are coordinated to the zinc ions, and two of the remaining three protonated. These exposed pyridine groups showed catalytic activity in the transesterification of ester **E** (Scheme 12). When racemic 1-phenyl-2-propanol was used, the ester product exhibited a modest ~8% ee in favor of the *S*-enantiomer.
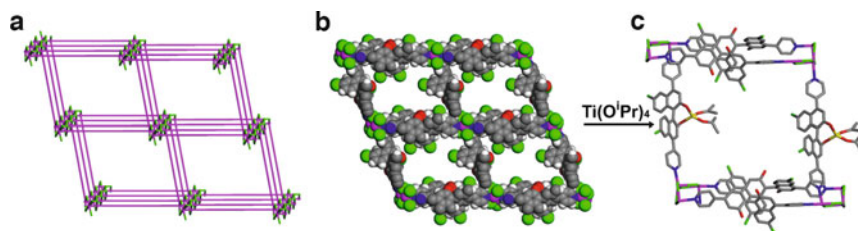
Fig. 16 (**a**) Schematic representation of the 3D framework of **14** showing the zigzag chains of [Cd $(\mu\text{-Cl})_2]_n$ along *a* axis. (**b**) Space-filling model of **14** as viewed down the *a* axis, showing large 1D chiral channel (1.6×1.8 nm). (**c**) Schematic representation of the active (BINOLate)Ti(O^{i}Pr)$_2$ catalytic sites in the open channels of **14**

Table 4 Ti(IV)-catalyzed ZnEt$_2$ additions to aromatic aldehydes[a]
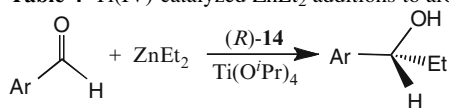
Ar	BINOL/Ti(O^{i}Pr)$_4$		14•Ti	
	conv.%	ee%	conv.%	ee%
1-Naph	>99	94	>99	93
Ph	>99	88	>99	83
4-Cl-Ph	>99	86	>99	80
3-Br-Ph	>99	84	>99	80
4'-G$_0$OPh	>99	80	>99	88
4'-G$_1$'OPh	>99	75	73	77
4'-G$_1$OPh	>99	78	63	81
4'-G$_2$'OPh	95[b]	67[b]	0	–
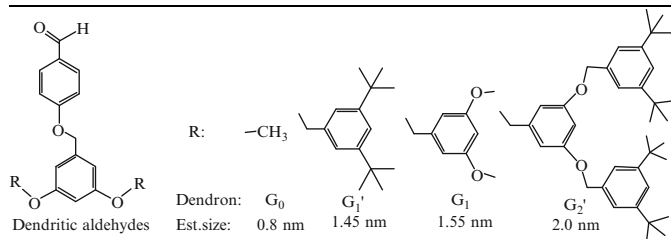
[a]All the reactions were conducted with 13 mol% of **14** or 20 mol% BINOL and excess amounts of Ti(O^{i}Pr)$_4$ at room temperature for 12 h. Conversions were determined by GC or NMR, while ee% values were determined on chiral GC or HPLC for all the secondary alcohols except for 4'-G$_2$'OPh whose ee% was determined by NMR spectrum of its Mosher's ester
[b]With 40 mol% BINOL

3.4 Postmodification of Homochiral MOFs Bearing Bridging Ligands with Orthogonal Functionalities

3.4.1 High Enantioselective Diethylzinc Addition Reactions

The Lin group used a postsynthetic modification strategy to generate a highly active and enantioselective heterogeneous catalyst from homochiral MOFs bearing bridging ligands with orthogonal functionalities. Slow vapor diffusion of diethyl ether into the mixture of (*R*)-6,6′-dichloro-2,2′-dihydroxyl-1,1′-binaphthyl-bipyridine (**L$_3$**) and CdCl$_2$ in DMF/MeOH led to 3D homochiral MOF [Cd$_3$(**L$_3$**)$_3$Cl$_6$]· 4DMF·6MeOH·3H$_2$O (**14**) [15]. The 3D framework structure of **14** resulted from linking 1D zigzag [Cd(μ-Cl)$_2$]$_n$ SBUs by the **L$_3$** ligands via pyridine coordination and had the largest channel opening of 1.6 × 1.8 nm running along the *a* axis (Fig. 16). More importantly, one third of the chiral dihydroxy groups in **14** are facing the open channels, which makes them accessible to secondary metal centers.

The porous solid **14** was pretreated by Ti(O^{i}Pr)$_4$ to generate the grafted Ti-BINOLate species. The resulting active "**14·Ti**" species efficiently catalyzed the diethylzinc addiction reactions in a level of ee (up to 93%) that is comparable to the homogeneous analogue (94% ee) (Table 4). The heterogeneous nature of this solid catalyst was confirmed by the nonreactive supernatant from a mixture of **14** and Ti (O^{i}Pr)$_4$. Moreover, a set of control experiments were performed using aldehydes
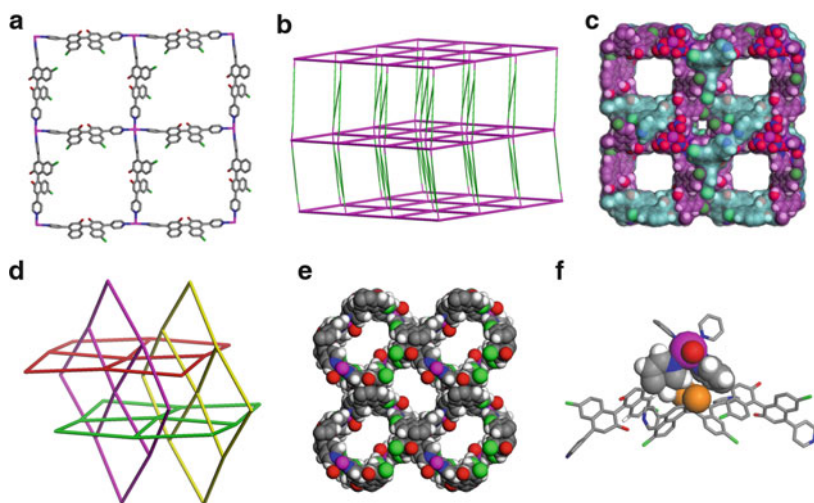

Fig. 17 (**a**) The 2D square grid in **15**. (**b**) Schematic representation of the 3D framework of **15**. (**c**) Space-filling model of **15** as viewed down the *c* axis, the twofold interpenetrating networks are shown with *blue and violet colors*. (**d**) Schematic representation of the interpenetration of mutually perpendicular 2D grids in **16**. (**e**) Space-filling model of **16** as viewed down the *c* axis. (**f**) Schematic representation of steric congestion around the chiral dihydroxyl group of **L$_3$** (*orange sphere*) arising from the interpenetration of mutually perpendicular 2D grids in **16**

with different size from 0.8 to 2.0 nm to show that the aldehydes are accessing the Ti active sites in the interior of crystals of **14**. Decreased conversion was found when larger aldehyde was used, and no conversion of aldehyde G_2' with size of 2.0 nm was used, which is larger than the size of the open channels of the framework. Such a size-dependant conversion further illustrated the heterogeneous nature of the **14**·Ti catalysts and that the catalytic reactions occur inside the open channels of the solid (instead of external surfaces of the solid).

3.4.2 Catalytic Activities Determined by Framework Structures

The chloride anions coordinate to the Cd centers to give $[Cd(\mu\text{-}Cl)_2]_n$ SBUs in **14**. It is well-established that the MOF structures critically depend on the anions used during the crystal growth. While using the same ligand L_3, Lin et al. obtained two different homochiral MOFs $[Cd_3(L_3)_4(NO_3)_6]\cdot7MeOH\cdot5H_2O$ (**15**) and $[Cd(L_3)_5(ClO_4)_2]\cdotDMF\cdot 4MeOH\cdot3H_2O$ (**16**) when $Cd(NO_3)_2$ and $Cd(ClO_4)_2$ were used as the metal sources [44]. Compound **15** shows twofold interpenetrated structure of two sets of 3D frameworks, which are constructed by 2D grids and 1D zigzag polymeric chains. Large channels with dimension of 13.5×13.5 Å exist along the c axis (Fig. 17c). Compound **16** adopts 3D network from highly interpenetrated 2D grids, resulting 1D channels with size of 1.2×1.5 nm (Fig. 17e).

Compound **15** was activated by $Ti(O^iPr)_4$ to lead to an active heterogeneous asymmetric catalyst for the diethylzinc addition to aromatic aldehydes with up to 90% ee. However, under the same conditions, a mixture of **16** and $Ti(O^iPr)_4$ was inactive in catalyzing the diethylzinc addition to aromatic aldehydes. Careful investigation of the structure of **16** revealed the close proximity of the Cd $(py)_2(H_2O)_2$ moiety in one 2D grid with the dihydroxyl groups of the other 2D grid, which made the dihydroxyl groups inaccessible to $Ti(O^iPr)_4$. When treated with $Ti(O^iPr)_4$, compounds **15** and **16** had entirely different activities due to the
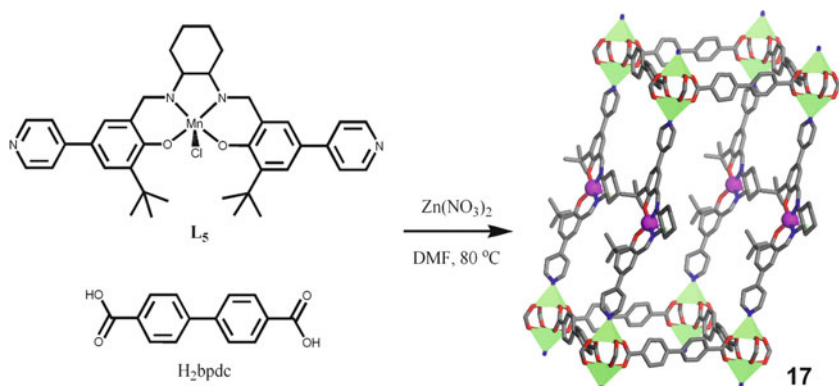
Scheme 13 Synthesis and framework structure of **17**
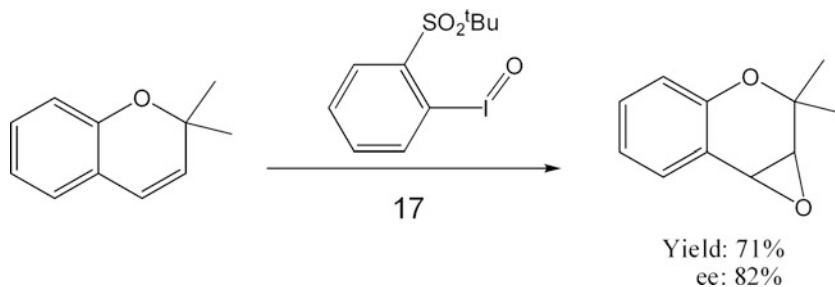
**Scheme 14** Asymmetric epoxidation catalyzed by **17**
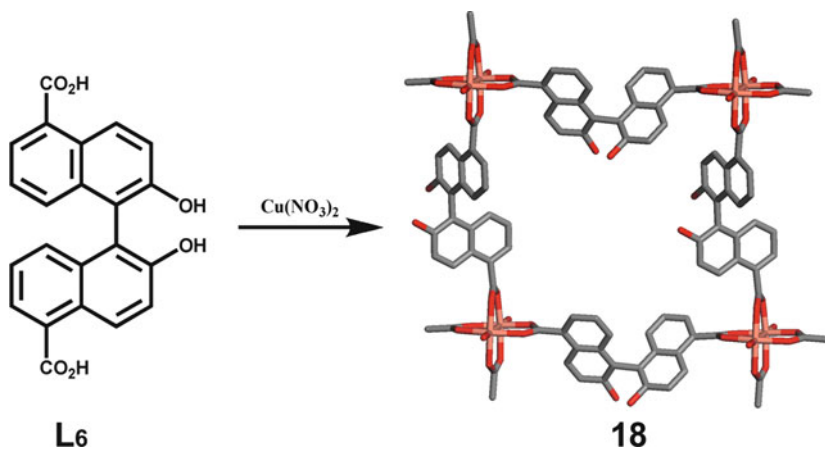
Scheme 15 Schematic representation of the synthesis of **18** and the connectivity of L_6 and copper paddle wheels

subtle structure differences. The finding of such a drastic difference in catalytic activity is remarkable since **15** and **16** were built from exactly the same building blocks, and this finding highlights the important role of the framework structure in determining the catalytic performance.

3.5 Homochiral MOFs with Precatalysts as Building Blocks

An alternative approach to catalytically active homochiral MOFs is to incorporate directly chiral metal complexes which are either active catalysts or precatalysts into the framework structures. For example, Hupp and coworkers have combined L_5 and H_2bpdc with $Zn(NO_3)_2$ and obtained twofold interpenetrating 3D networks $[Zn_2(bpdc)_2L_5] \cdot 10DMF \cdot 8H_2O$ (**17**) (Scheme 12) [46]. While the channels along
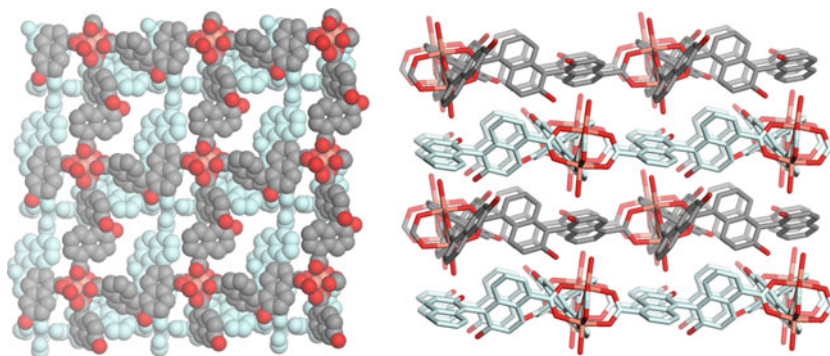
Fig. 18 Space-filled model of **18** as viewed down the *b* axis (left) and the stacking patterns of 2D grids as viewed along the *c* axis

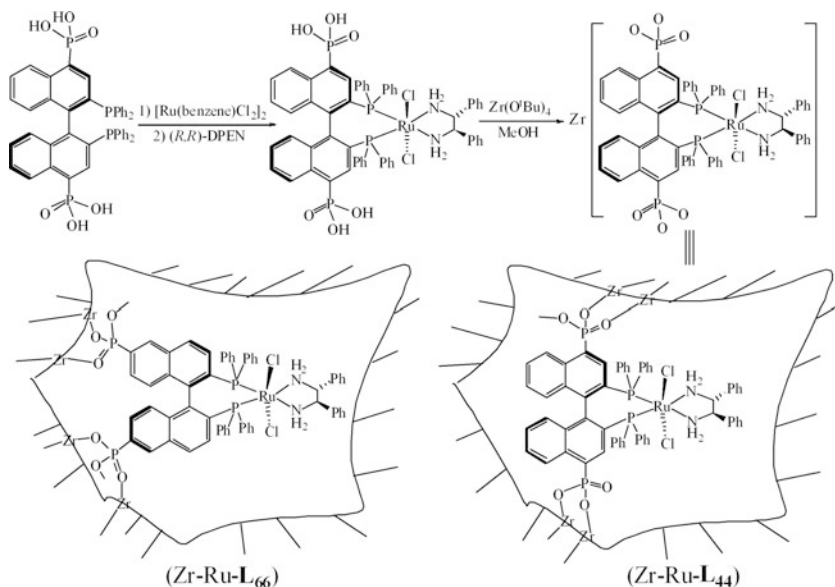**Table 5** Asymmetric ring-opening reaction of epoxide with amine
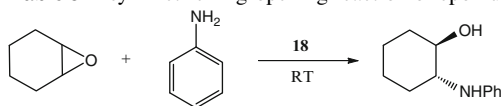
Catalyst	Solvent	Time/h	Yield (%)	ee (%)
18	Toluene	48	54	45
18	None	24	51	51
(*S*)-BINOL	None	24	3	2

the *b* axis are blocked as the result of interpenetration, channels in the *a* and *c* directions still remain with size of 6.2 × 6.2 Å and 6.2 × 15.7 Å, respectively (Scheme 13).

The orientation of **L₅** in the frameworks makes all Mn(III) sites accessible through the channels. The resulting open frameworks with built-in (salen)Mn complexes showed catalytic activity towards asymmetric olefin epoxidation reactions. In the asymmetric epoxidation of 2,2-dimethyl-2*H*-chromene catalyzed by **17** (Scheme 14), 71% yield and 82% ee were obtained. No significant decrease of catalyst activity was observed during the reaction and the catalyst could be recycled and reused several times. Notably, the heterogeneous catalyst **17** has shown higher activity than the homogeneous counterpart, albeit with slightly lower ee.

Using a similar approach to the Lin group, Tanaka and coworkers synthesized homochiral MOFs [Cu₂(**L₆**)₂(H₂O)₂]MeOH.H₂O (**18**) from 2,2′-dihydroxyl-1,′1-binaphthyl-5,5′-dicaroxylatic acid (**L₆**) and Cu(NO₃)₂ [45]. The copper paddlewheel SBUs in **18** were linked by BINOL scaffolds through 5,5′ positions (Scheme 15). The resulting 2D square grid networks are stacked along the *b* axis with a interlayer Cu–Cu distance of 15.6 Å (Fig. 18).

Scheme 16 Schematic representation of formation of zirconium phosphonate-based chiral porous hybrid materials

The homochiral framework **18** is capable of catalyzing the asymmetric ring-opening of epoxides with amines. Compound **18** shows moderate catalytic activity with up to 54% yield and 51% ee (Table 5). The control experiments were carried by using S-BINOL as catalyst, and only negligible yield and ee were obtained. The mechanism for this reaction however remained unclear.

Lin and coworkers have reported zirconium phosphonate-derived Ru-BINAP systems (Scheme 16) [49]. Zirconium phosphonate-based chiral porous hybrid materials containing the Ru(BINAP)(diamine)Cl$_2$ precatalysts showed excellent enantioselectivity (up to 99.2% ee) in the asymmetric hydrogenation of aromatic ketones. These catalysts were also readily recovered by centrifugation and reused for up to 10 times without significant loss of catalyst activity and enantioselectivity. Related zirconium phosphonates containing Ru(BINAP)(DMF)$_2$Cl$_2$ precatalysts were successfully used for asymmetric hydrogenation of β-keto esters with up to 95% ee [50].

4   Conclusions and Perspectives

This chapter has summarized recent developments in the rational design of catalytically active MOFs. Their applications in both achiral and asymmetric catalysis were surveyed. Three distinct approaches have been developed to construct catalytically MOFs, including the use of unsaturated metal-connecting points as catalytic centers, the use of functional groups in the bridging ligands as active sites, and the entrapment of catalytically active species inside the channels and pores of MOFs. The use of channels and pores in MOFs as hosts for size- and shape-selective reactions was also discussed. Limited thermal and hydrolytic stabilities of MOFs however present major hurdles for their practical applications in achiral catalysis, particularly for the reactions that can be effectively catalyzed by microporous inorganic oxides such as zeolites. Homochiral MOFs on the other hand can be used as heterogeneous catalysts for stereoselective reactions which cannot be catalyzed by zeolites. Compared to the MOFs available for achiral catalysis, only a very small number of homochiral MOFs have so far been developed for heterogeneous asymmetric catalysis due to the challenge in designing homochiral MOFs with large enough open channels to allow the access of typically large prochiral reagents. Research on asymmetric catalysis using homochiral MOFs has barely scratched the surface. Many more catalytically active systems will be developed and used for stereoselective organic transformations in the coming years.

References

 1. Batten SR, Robson R (1998) Angew Chem Int Ed 37:1460
 2. Moulton B, Zaworotko MJ (2001) Chem Rev 101:1629
 3. Evans OR, Lin W (2002) Acc Chem Res 35:511
 4. Ferey G, Mellot-Draznieks C, Serre C, Millange F (2005) Acc Chem Res 38:217
 5. Yaghi OM, O'Keeffe M, Ockwig NW, Chae HK, Eddaoudi M, Kim J (2003) Nature 423:705
 6. Hill RJ, Long DL, Champness NR, Hubberstey P, Schroder M (2005) Acc Chem Res 38:335
 7. Bradshaw D, Warren JE, Rosseinsky MJ (2007) Science 315:977
 8. Rosi NL, Eckert J, Eddaoudi M, Vodak DT, Kim J, O'Keeffe M, Yaghi OM (2003) Science 300:1127
 9. Kesanli B, Cui Y, Smith MR, Bittner EW, Bockrath BC, Lin W (2005) Angew Chem Int Ed 44:72
10. Chen B, Zhao X, Putkham A, Hong K, Lobkovsky EB, Hurtado EJ, Fletcher AJ, Thomas KM (2008) J Am Chem Soc 130:6411
11. Pan L, Parker B, Huang X, Olson DH, Lee JY, Li J (2006) J Am Chem Soc 128:4180
12. Evans OR, Ngo HL, Lin WB (2001) J Am Chem Soc 123:10395
13. Han JW, Hill CL (2007) J Am Chem Soc 129:15094

14. Hasegawa S, Horike S, Matsuda R, Furukawa S, Mochizuki K, Kinoshita Y, Kitagawa S (2007) J Am Chem Soc 129:2607
15. Wu CD, Hu A, Zhang L, Lin WB (2005) J Am Chem Soc 127:8940
16. Hwang YK, Hong DY, Chang JS, Jhung SH, Seo YK, Kim J, Vimont A, Daturi M, Serre C, Ferey G (2008) Angew Chem Int Ed 47:4144
17. Schroeder F, Esken D, Cokoja M, van den Berg MWE, Lebedev OI, van Tendeloo G, Walaszek B, Buntkowsky G, Limbach HH, Chaudret B, Fischer RA (2008) J Am Chem Soc 130:6119
18. Fujita M, Kwon YJ, Washizu S, Ogura K (1994) J Am Chem Soc 116:1151
19. Ohmori O, Fujita M (2004) Chem Commun 14:1586
20. Schlichte K, Kratzke T, Kaskel S (2004) Microporous Mesoporous Mat 73:81
21. Chui SSY, Lo SMF, Charmant JPH, Orpen AG, Williams ID (1999) Science 283:1148
22. Horike S, Dinca M, Tamaki K, Long JR (2008) J Am Chem Soc 130:5854
23. Alaerts L, Seguin E, Poelman H, Thibault-Starzyk F, Jacobs PA, De Vos DE (2006) Chem Eur J 12:7353
24. Striegler S (2006) Tetrahedron 62:9109
25. Kato CN, Hasegawa M, Sato T, Yoshizawa A, Inoue T, Mori W (2005) J Catal 230:226
26. Dybtsev DN, Nuzhdin AL, Chun H, Bryliakov KP, Talsi EP, Fedin VP, Kim K (2006) Angew Chem Int Ed 45:916
27. Gomez-Lor B, Gutierrez-Puebla E, Iglesias M, Monge MA, Ruiz-Valero C, Snejko N (2002) Inorg Chem 41:2429
28. Perles J, Iglesias M, Martin-Luengo MA, Monge MA, Ruiz-Valero C, Snejko N (2005) Chem Mat 17:5837
29. Ferey G, Mellot-Draznieks C, Serre C, Millange F, Dutour J, Surble S, Margiolaki I (2005) Science 309:2040
30. Pan L, Liu HM, Lei XG, Huang XY, Olson DH, Turro NJ, Li J (2003) Angew Chem Int Ed 42:542
31. Turro NJ (2000) Acc Chem Res 33:637
32. Uemura T, Kitaura R, Ohta Y, Nagaoka M, Kitagawa S (2006) Angew Chem Int Ed 45:4112
33. Uemura T, Ono Y, Kitagawa K, Kitagawa S (2008) Macromolecules 41:87
34. Uemura T, Kitagawa K, Horike S, Kawamura T, Kitagawa S, Mizuno M, Endo K (2005) Chem Commun 48:5968
35. Uemura T, Hiramatsu D, Kubota Y, Takata M, Kitagawa S (2007) Angew Chem Int Ed 46:4987
36. Ezuhara T, Endo K, Aoyama Y (1999) J Am Chem Soc 121:3279
37. Wu ST, Wu YR, Kang QQ, Zhang H, Long LS, Zheng ZP, Huang RB, Zheng LS (2007) Angew Chem Int Ed 46:8475
38. Kepert CJ, Prior TJ, Rosseinsky MJ (2000) J Am Chem Soc 122:5158
39. Bradshaw D, Prior TJ, Cussen EJ, Claridge JB, Rosseinsky MJ (2004) J Am Chem Soc 126:6106
40. Lin Z, Slawin AMZ, Morris RE (2007) J Am Chem Soc 129:4880
41. Seo JS, Whang D, Lee H, Jun SI, Oh J, Jeon YJ, Kim K (2000) Nature 404:982
42. Ngo HL, Lin WB (2002) J Am Chem Soc 124:14298
43. Wu CD, Lin WB (2005) Angew Chem Int Ed 44:1958
44. Wu C, Lin W (2007) Angew Chem Int Ed 46:1075
45. Tanaka K, Oda S, Shiro M (2008) Chem Commun 820
46. Cho SH, Ma BQ, Nguyen ST, Hupp JT, Albrecht-Schmitt TE (2006) Chem Commun 2563
47. Berthod M, Mignani G, Woodward G, Lemaire M (2005) Chem Rev 105:1801
48. Miyashita A, Yasuda A, Takaya H, Toriumi K, Ito T, Souchi T, Noyori R (1980) J Am Chem Soc 102:7932
49. Hu AG, Ngo HL, Lin WB (2003) J Am Chem Soc 125:11490
50. Hu AG, Ngo HL, Lin WB (2004) Angew Chem Int Ed 43:2501
51. Cejka J, Wichterlova B (2002) Catal Rev Sci Eng 44:375